The effect of three-dimensional fields on bounce averaged particle drifts in a tokamak

C. C Hegna
Departments of Engineering Physics and Physics,
University of Wisconsin-Madison, Madison, WI 53706

The impact of applied 3D magnetic fields on the bounce-averaged precessional drifts in a tokamak plasma are calculated. Local 3D MHD equilibrium theory is used to construct solutions to the equilibrium equations in the vicinity of a magnetic surface for a large aspect ratio circular tokamak perturbed by applied 3D fields. Due to modulations of the local shear caused by near-resonant Pfirsch-Schlüter currents, relatively weak applied 3D fields can have a large effect on trapped particle precessional drifts. **Pacs. nos. 52.20.Dq, 52.35.Qz, 52.55.Dy**

I. INTRODUCTION

Applying three-dimensional (3D) magnetic fields to otherwise axisymmetric toroidal confinement devices affects a number of plasma physics properties [1, 2]. In particular, 3D fields whose resonant surface lies in the edge region of H-mode tokamaks can suppress edge localized modes (ELMs) under certain conditions [3–7]. The precise mechanism for this suppression is not known but is likely tied to a change in the transport properties in the edge region. Stochastic transport due to overlapped magnetic islands is not thought to be operable throughout the pedestal due to the presence of plasma flows that shield the penetration of externally applied 3D fields [8–10]. However, even with plasma shielding, applied 3D fields can significantly distort the shape of the magnetic surfaces [11] and affect MHD stability [12–14]. The sensitivity of local MHD stability to 3D shaping suggests that microinstability properties are also affected by applied 3D fields. Indeed, turbulent fluctuation measurements in the DIII-D edge show a dependency on the applied 3D fields [15]. Trapped particles modes are one of many candidates to explain turbulent transport in the pedestal region [16–20]. In the following, the effect of applied 3D fields on trapped particle drifts in a tokamak is investigated as a precursor to studies of 3D effects on trapped particle mode turbulence.

Regions of unfavorable curvature can lead to instability in the presence of trapped particles [21, 22]. Trapped-particle mode stability depends upon the relative sign of the bounce-averaged trapped particle drift and the driving thermodynamic gradient. While deeply trapped particles are destabilizing in a tokamak, precise details of the trapped particle drive depend upon the properties of the MHD equilibrium. Indeed, in the high β limit, pressure induced Pfirsch-Schlüter currents produce modulations to the local shear that tend to reverse the direction of the precession drift [23], This is a stabilizing effect for collisionless trapped particle modes in tokamaks.

In order to understand how 3D shaping can influence trapped particle drifts, a solution to the 3D MHD equilibrium equations is required. Understanding the plasma response to applied 3D fields is a topic of considerable interest to the plasma community with a variety of tools being used to describe the resultant 3D steady state [24, 25]. In particular, quantification of shielding physics via plasma rotation generally depends upon non-ideal MHD physics. However, since local stability calculations only require knowledge of the equilibrium quantities in a flux tube, it is not necessary to construct "global" solutions that account for shielding physics at rational surfaces. In this work, the existence of a topologically toroidal magnetic surface is presumed away from magnetic field resonances. The procedure outlined in Ref. [13] is utilized whereby a 3D equilibrium local to a magnetic surface [26] is constructed assuming a small 3D distortion away from a lowest order axisymmetric equilibrium. In this formulation, the shape of the magnetic surface is denoted by the mapping function $\mathbf{X}(\theta,\zeta)$ on the magnetic surface labeled by the poloidal flux function $\psi=\psi_o$ where θ and ζ are the straight-field line poloidal and toroidal angles. From $\mathbf{X}$ and the field line pitch $q(\psi_o)$, various geometric quantities associated with the field line can be constructed. Despite the rather small values of applied 3D magnetic field used in present day tokamak experiments, these can produce important modifications to stability quantities and are sensitive to pitch resonant components of the field shaping [31]. Modulations of the local shear due to near-resonant Pfirsch-Schlüter currents can play an important role in high pressure gradient regions and produce notable changes to infinite-n ideal ballooning stability properties [13]. Because of the sensitivity of the trapped particles to the magnetic field properties and the local shear in particular, trapped particle instabilities can also be significantly affected by applied 3D fields.

In Sec. II, we provide a brief review of local 3D MHD equilibrium theory. In Section III, we apply the equilibrium model to derive an expression for the trapped particle precessional drift. The calculation is specialized to consider the case of a high aspect ratio circular flux surface perturbed by a weak 3D field. A brief summary is provided in Section IV.

II. LOCAL 3D MHD EQUILIBRIUM

A description of the equilibrium in the presence of an applied 3D magnetic field can be provided by local 3D MHD equilibrium theory [26, 27]. In this formulation equilibrium quantities on a topologically toroidal mag-

netic surface are uniquely determined by the shape of the magnetic surface parameterized by two straight-field line angles, the value of the safety factor q and two profile quantities. This technique is the 3D generalization of the widely used "Miller equilibrium" which describes local solutions of the Grad-Shafranov equation for 2D configurations [28]. Local 3D equilibrium theory has been employed to quantify proximity to ballooning stability boundaries in stellarator experiments [29, 30].

Equilibrium properties are sought on the single magnetic surface $\psi = \psi_o$. In the vicinity of $\psi = \psi_o$, the magnetic field mapping can be written

$$\mathbf{X}(\psi,\theta,\zeta) = \mathbf{x}(\psi_o,\theta,\zeta) + (\psi-\psi_o)\frac{\partial \mathbf{x}}{\partial \psi}(\psi_o,\theta,\zeta) + ...$$

$$= \mathbf{x}_0 + (\psi-\psi_o)\mathbf{x}_o' + ... \quad (1)$$

where θ and ζ are straight field line poloidal and toroidal angles, respectively and ψ is the poloidal flux function. From $\mathbf{x}_o$ and $\mathbf{x}_o'$ all components of $\mathbf{B}$ and $\mathbf{J}$ can be determined on the magnetic surface of interest. From the first term in Eq. (1), expressions for the unit parallel and normal vectors can be calculated

$$\hat{\mathbf{b}} = \frac{q\frac{\partial \mathbf{X}}{\partial \zeta} + \frac{\partial \mathbf{X}}{\partial \theta}}{(q^2 g_{\zeta\zeta} + 2q g_{\zeta\theta} + g_{\theta\theta})^{1/2}}, \quad (2)$$

$$\hat{\mathbf{n}} = \frac{\frac{\partial \mathbf{X}}{\partial \theta}\times\frac{\partial \mathbf{X}}{\partial \zeta}}{(g_{\zeta\zeta}g_{\theta\theta} - g_{\zeta\theta}^2)^{1/2}}, \quad (3)$$

where $g_{\zeta\zeta} = \partial \mathbf{x}_o/\partial\zeta \cdot \partial \mathbf{x}_0/\partial\zeta, g_{\zeta\theta} = \partial \mathbf{x}_0/\partial\zeta \cdot \partial \mathbf{x}_0/\partial\theta$ and $g_{\theta\theta} = \partial \mathbf{x}_o/\partial\theta \cdot \partial \mathbf{x}_0/\partial\theta$. Derivatives of the orthonormal basis set $\hat{\mathbf{b}}$, $\hat{\mathbf{n}}$ and $\hat{\mathbf{b}}\times\hat{\mathbf{n}}$ along the field line produce a variant of Frenet's formulae

$$(\hat{\mathbf{b}}\cdot\nabla)\hat{\mathbf{b}} = \kappa_n\hat{\mathbf{n}} + \kappa_g\hat{\mathbf{b}}\times\hat{\mathbf{n}}, \quad (4)$$

$$(\hat{\mathbf{b}}\cdot\nabla)\hat{\mathbf{n}} = -\kappa_n\hat{\mathbf{b}} + \tau_n\hat{\mathbf{b}}\times\hat{\mathbf{n}}, \quad (5)$$

$$(\hat{\mathbf{b}}\cdot\nabla)(\hat{\mathbf{b}}\times\hat{\mathbf{n}}) = -\tau_n\hat{\mathbf{n}} - \kappa_g\hat{\mathbf{b}}, \quad (6)$$

where κ_n (normal curvature), κ_g (geodesic curvature) and τ_n (normal torsion) describe the geometric properties of the field lines. The constraint $\hat{\mathbf{n}}\cdot\mathbf{J} = 0$ for the current profile $\mathbf{J}$ provides a first order partial differential equation for the Jacobian $\sqrt{g}$

$$\frac{\partial}{\partial\theta}\frac{q g_{\zeta\zeta} + g_{\zeta\theta}}{\sqrt{g}} = \frac{\partial}{\partial\zeta}\frac{q g_{\theta\zeta} + g_{\theta\theta}}{\sqrt{g}}, \quad (7)$$

whose solution can be used to calculate the equilibrium magnetic field $\mathbf{B} = (q\partial\mathbf{x}_o/\partial\zeta + \partial\mathbf{x}_o/\partial\theta)/\sqrt{g} = q\nabla\psi\times\nabla\theta + \nabla\zeta\times\nabla\psi$ and $\nabla\psi = (\partial\mathbf{x}_o/\partial\theta\times\partial\mathbf{x}_o/\partial\zeta)/\sqrt{g}$ at the magnetic surface $\psi = \psi_o$.

The components of $\mathbf{x}_o'$ are determined by solutions to the ideal MHD equilibrium equations in the vicinity of the magnetic surface and are uniquely determined with the specification of two flux functions, typically the pressure gradient ($p' = dp/d\psi$) and the safety factor gradient, ($q' = dq/d\psi$). $\mathbf{x}_o'$ can be written

$$\mathbf{x}_0' = \frac{1}{|\nabla\psi|}\hat{\mathbf{n}} + h\mathbf{B} + D\frac{|\nabla\psi|}{B}\hat{\mathbf{b}}\times\hat{\mathbf{n}}. \quad (8)$$

The quantity of interest in many local stability analyses [13, 32–34] is the quantity D that denotes the variation of the local shear. The local shear $s = \hat{\mathbf{b}}\times\hat{\mathbf{n}}\cdot\nabla\times(\hat{\mathbf{b}}\times\hat{\mathbf{n}})$ is related by the vector identity $s = \mu_o J_{||}/B - 2\tau_n$ [26]. This relation provides an expression for D given by

$$-\frac{q'}{\sqrt{g}} + \mathbf{B}\cdot\nabla D = \frac{B^2}{|\nabla\psi|^2}(\sigma + p'\lambda - 2\tau_n), \quad (9)$$

where the parallel current can be decomposed into the flux surface averaged current

$$\sigma = \mu_o\frac{<\mathbf{J}\cdot\mathbf{B}>}{<B^2>}, \quad (10)$$

and Pfirsch-Schlüter current proportional to the geometric factor λ calculated from the magnetic differential equation

$$\mathbf{B}\cdot\nabla\lambda = 2\kappa_g\mu_o\frac{|\nabla\psi|}{B}, \quad (11)$$

subject to $<\lambda B^2> = 0$. The flux surface average of Eq. (9) produces an identity that relates q', p' and σ. The quantity h in Eq. (9) is similarly governed by a magnetic differential equation with source terms driven by p', q' and magnetic geometry. In the axisymmetric limit, h is directly proportional to D and given by the relation $h = Dg^{\psi\psi}\sqrt{g}/qR^2B^2$ [26]. The specification of $\mathbf{x}_o$, q and two profile quantities on a flux surface completely describes the equilibrium quantities locally.

III. PRECESSION FREQUENCY OF TRAPPED PARTICLES

The crucial quantity for trapped particle modes is the precession frequency of a trapped particle which for a tokamak can be written

$$<\omega_D> = k_\alpha <\mathbf{v}_D\cdot\nabla\alpha> = \frac{1}{e}\frac{\partial J}{\partial\psi}(\frac{\partial J}{\partial K})^{-1}, \quad (12)$$

for perpendicular wavenumber k_α. The longitudinal invariant involves an integral over the trapped particle bounce motion

$$J = \int m v_{||} dl = \int m v_{||} B\sqrt{g}\, d\theta, \quad (13)$$

where θ labels points along the field-line labeled by poloidal flux ψ and field-line label $\alpha = q\theta - \zeta$. Here $v_{||}^2 = v^2 - 2\mu B/m$ for particle energy $K = mv^2/2$ and magnetic moment μ and

$$\frac{\partial J}{\partial\psi} = m\int d\theta\, v_{||}[\frac{\partial(B\sqrt{g})}{\partial\psi} - \frac{\mu B\sqrt{g}}{v_{||}^2}\frac{\partial B}{\partial\psi}], \quad (14)$$

$$\frac{\partial J}{\partial K} = \int d\theta\, \frac{B\sqrt{g}}{v_{||}}. \quad (15)$$

Using local 3D equilibrium theory to work out the important elements of the integrand, one finds

$$\frac{1}{\sqrt{g}B}\frac{\partial}{\partial\psi}(\sqrt{g}B) = \frac{1}{q}\frac{dq}{d\psi}\frac{B_\zeta B^\zeta}{B^2} - \frac{\kappa_n}{|\nabla\psi|} - D\kappa_g\frac{|\nabla\psi|}{B}$$

$$+\frac{1}{B}\mathbf{B}\cdot\nabla(hB), \tag{16}$$

$$\frac{1}{B}\frac{\partial B}{\partial\psi} = \frac{\kappa_n}{|\nabla\psi|} + D\kappa_g\frac{|\nabla\psi|}{B} - \frac{\mu_o}{B^2}\frac{dp}{d\psi} + \frac{h}{B}\mathbf{B}\cdot\nabla B, \tag{17}$$

where $B_\zeta = \mathbf{B}\cdot\partial\mathbf{x}_o/\partial\zeta$ and $B^\zeta = \mathbf{B}\cdot\nabla\zeta = q/\sqrt{q}$. The terms proportional to h in these expressions are generally $\mathcal{O}(B_\theta B^\theta/B_\zeta B^\zeta) \sim \mathcal{O}(\epsilon^2/q^2)$ smaller than the largest terms in each of these expressions. As such, we drop these terms in the following and derive

$$\frac{\partial J}{\partial\psi} = m\int d\theta\ \sqrt{g}B[v_{||}\frac{q'}{q}$$

$$-(v_{||} + \frac{\mu B}{v_{||}})(\frac{\kappa_n}{|\nabla\psi|} + D\kappa_g\frac{|\nabla\psi|}{B}) + \frac{\mu B}{v_{||}}\frac{\mu_o p'}{B^2}], \tag{18}$$

For a large aspect ratio approximation, we make use of $B = B_o/(1+\epsilon\cos\theta)$ to parameterize velocity space using v^2 and pitch angle variable k^2 defined by

$$k^2 = \frac{1}{2}(\frac{1-2\mu B_o/mv^2}{\epsilon} + 1). \tag{19}$$

Trapped particles are defined by $0 \le k^2 \le 1$ with the trapped passing boundary at $k^2 = 1$. In the small $\epsilon \ll 1$ limit, we have the approximate expression $v_{||} \approx v\sqrt{2\epsilon}\sqrt{k^2 - \sin^2\theta/2}$. In the large aspect ratio circular flux surface limit ($R = R_o + r\cos\theta$, $Z = r\sin\theta$, $\epsilon = r/R_o \ll 1$), the geometric coefficients are given by the approximate formulae,

$$\frac{\kappa_n}{|\nabla\psi|} = -\frac{q\cos\theta}{B_o r R_o}, \tag{20}$$

$$\frac{\kappa_g|\nabla\psi|}{B} = \frac{r\sin\theta}{qR}, \tag{21}$$

$$\lambda = -\frac{2\mu_o r}{B_o}\cos\theta. \tag{22}$$

The two profiles p' and q' are related to the dimensionless quantities s and α

$$q' = \frac{q^2}{B_o r^2}s, \tag{23}$$

$$2\mu_o p' = -\frac{B_o}{qrR_o}\alpha, \tag{24}$$

and the variation of the local shear is given by

$$D = \alpha\frac{q^2}{B_o r^2}\sin\theta, \tag{25}$$

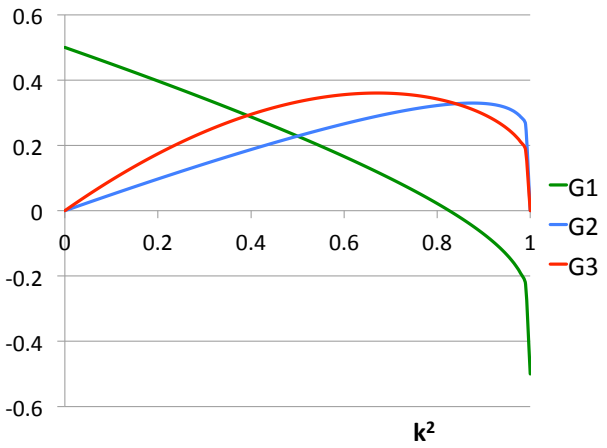

FIG. 1. The three contributions to the precessional drift formula Eq. (26) are plotted as a function of pitch angle variable

With the insertion of these expressions in Eq. (18) the classic results from Connor et al [23] are reproduced.

$$< \omega_D >= k_\alpha\frac{qmv^2}{eB_o r R_o}(G_1 - \frac{\alpha}{4q^2} + 2sG_2 - \alpha G_3), \tag{26}$$

where

$$G_1 = \frac{E(k)}{K(k)} - \frac{1}{2}, \tag{27}$$

$$G_2 = \frac{E(k)}{K(k)} + k^2 - 1, \tag{28}$$

$$G_3 = \frac{2}{3}[\frac{E(k)}{K(k)}(2k^2-1) + 1 - k^2]. \tag{29}$$

The three quantities G_1, G_2 and G_3 are plotted as a function of pitch angle variable in Figure 1. The term proportional to G_1 in Eq. (26) is due to the normal curvature and dominates for deeply trapped particles (small values of k^2). Positive values of the averaged shear ($s > 0$) increase $< \omega_D >$ whereas pressure gradients tend to reduce the precession frequency through two effects. The term proportional to $-(\alpha^2/4q^2)$ is due to the diamagnetic effect [35] while the term scaling with $-\alpha G_3$ is due to the variation of local shear (proportional to the quantity D) caused by the Pfirsch-Schlüter current [23]. As noted previously, large values of α can reverse the direction of $< \omega_D >$ and provide a stabilizing contribution to trapped particle instabilities in tokamaks.

The effect of an applied 3D field can be modeled in the same fashion as in Ref. [13]. Specifically, we can write the fiux surface parametrization

$$R = R(\theta) + \sum_i \gamma_i\cos(M_i\theta - N_i\zeta), \tag{30}$$

$$Z = Z(\theta) + \sum_i \gamma_i\sin(M_i\theta - N_i\zeta) \tag{31}$$

where $R(\theta)$ and $Z(\theta)$ are inverse mapping coordinates for the axisymmetric equilibrium, θ is the straight field-line poloidal angle for the axisymmetric equilibrium and ζ is the geometric toroidal angle. Assuming the 3D components are small, the quantities γ_i are linearly related to the 3D magnetic fields via a coupling matrix [31]. Corrections to various geometric coefficients due to the 3D fields can be calculated using the above parameterization. In the large aspect ratio circular flux surface limit, one finds the following key set of geometric coefficients

$$\kappa_n = -\frac{\cos\theta}{R_o} - \sum_i M_i \frac{\gamma_i}{r R_o}\cos(M_i\theta - N_i\zeta), \tag{32}$$

$$\kappa_g = \frac{\sin\theta}{R_o} + \sum_i M_i \frac{\gamma_i}{r R_o}\sin(M_i\theta - N_i\zeta), \tag{33}$$

$$\lambda = -2\mu_o \frac{r}{B_o}[\cos\theta + \sum_i \frac{M_i}{M_i - N_i q}\frac{\gamma_i}{r}\cos(M_i\theta - N_i\zeta)] \tag{34}$$

where the first term in each expression is the conventional high-aspect ratio prediction and the last term is the leading contribution resulting from the 3D distortion. The 3D fields produce $\mathcal{O}(M_i\gamma_i/r)$ corrections to the curvature vector. The expression for the Pfirsch-Schlüter coefficient contains quantities that become large near rational values of q. This produces important corrections to $< \omega_D >$ through the modification of the variation of the local shear. Assuming the dominant effect of the 3D field are order unity corrections to the Pfirsch-Schlüter coefficient Eq. (9), Eq. (18) and Eq. (34) can be used to calculate the 3D correction to $< \omega_D >$ given by

$$< \omega_D >= k_\alpha \frac{qmv^2}{eB_o r R_o}[G_1 - \frac{\alpha}{4q^2} + 2sG_2 - \alpha G_3$$

$$+2\alpha G_2 \sum_i \frac{M_i}{M_i - N_i q}\frac{\gamma_i}{r}\delta_i \cos(N_i\alpha)], \tag{35}$$

where

$$\delta_i = \frac{\int d\theta\ v_{||}\cos(M_i - N_i q)\theta}{\int d\theta\ v_{||}}. \tag{36}$$

Note the expression from the 3D correction explicitly depends upon the field line label $\alpha = q\theta - \zeta$. This indicates the bounce averaged particle drifts are field line dependent and hence can lead to different trapped particle mode behavior on different flux tubes within the same surface. The additional dependence on field line label is a notable feature of local mode stability in 3D configurations using ballooning formalism [36] and a known property of microinstabilities (including trapped particle modes) in stellarators [37–40]. To demonstrate the effect of the 3D field, a plot of $< \omega_D > /\omega_o$ ($\omega_o = k_\alpha q m_s v^2/e_s B_o r R_o$) versus pitch angle variable is shown in Figure 2 using the parameters $\alpha = 2, s = 2$ in Eq. (35) assuming a single dominant harmonic in the sum over

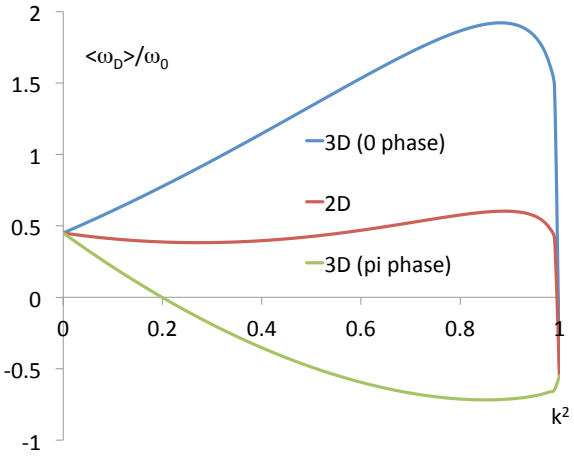

FIG. 2. The precessional drift formula Eq. (35) is plotted as a function of pitch angle variable. The precessional drift is normalized to $\omega_o = k_\alpha q m_s v^2/e_s B_o r R_o$. A single 3D contribution to the formula is included using the parameters $s = 2, \alpha = 2, \gamma/r = 0.01, M = 10, M - Nq = 0.1$. The three curves correspond to the field line choice $\cos(N\alpha) = 1$ (0 phase), $\cos(N\alpha) = 0$ (2D) and $\cos(N\alpha) = -1$ (pi phase).

3D components with $\gamma/r = 0.01, M = 10, M - Nq = 0.1$. The top curve in this plot correspond to the field line choice $\cos(N\alpha) = 1$, the middle curve corresponds to $\cos(N\alpha) = 0$ (no 3D effect) and the bottom curve corresponds to the field line choice $\cos(N\alpha) = -1$. Clearly, within the context of this simple limit, the 3D distortion can have a substantial effect on trapped particle orbits. For the case with a 3D field on the field line choice $\cos(N\alpha) = -1$ only the deeply trapped particles have precession frequencies that are destabilizing. Due to the 3D field, it's likely the trapped particle mode response will be highly field line dependent.

An additional complication brought about by 3D fields is the generation of bounce averaged net radial drift of trapped particles. For the case with finite radial wave vector, the relevant frequency is given by

$$< \omega_D >= k_\alpha < \mathbf{v}\cdot\nabla\alpha > + k_\psi < \mathbf{v}\cdot\nabla\psi >$$

$$= k_\alpha \frac{1}{e}(\frac{\partial J}{\partial K})^{-1}(\frac{\partial J}{\partial \psi} - \frac{k_\psi}{k_\alpha}\frac{\partial J}{\partial \alpha}). \tag{37}$$

The additional contribution scales with α dependence of B ($\partial B/\partial\alpha \sim N_i\delta_i$) and provides a contribution to trapped particle motion in the presence of finite k_ψ. Additionally, net radial banana drifts produce a mechanism to collisionlessly damp zonal flows [41]. In this work, the effect of a radial electric field has been neglected for simplicity. The presence of radial electric fields are known to produce a number of effects on trapped particle motion and associated neoclassical transport in 3D systems

[42–44]. Moreover, applied 3D fields in tokamaks also alter neoclassical transport through passing particle effects and the generation of super-bananas orbits [45]. All of these effects will need to be accounted for when deducing the net effect of 3D fields on trapped particle mode turbulence.

IV. SUMMARY

The effects of applied 3D magnetic fields on the bounce-averaged precessional drifts in tokamak plasma are calculated. Local 3D MHD equilibrium theory is employed to construct local solutions to the equilibrium equations perturbed by applied 3D fields. Assuming the applied fields are small, a perturbation approach is employed to construct changes in various geometric quantities due to the 3D fields. A prominent feature of the 3D equilibrium is the production of substantial non-axisymmetric modulation of the Pfirsch-Schlüter current spectrum and local magnetic shear. This modulation is present even when shielding physics is operative to prevent the formation of magnetic islands. This effect is due to a near pitch resonance between the field line and the the 3D distortion of the magnetic surface. As shown in Eqs. (12) and (18), modulations in the local shear can introduce prominent corrections to the precession drift properties of trapped electrons. In order to gain analytic insight, formulas corresponding to the case of large aspect ratio, circular flux surface tokamak perturbed by a weak 3D field are derived for the precessional drift and given in Eq. (35).

The calculation presented here parallels previous efforts to use local 3D equilibrium theory to deduce the effects of small 3D distortions on ideal MHD ballooning MHD instabilities [13, 31]. Three-dimensional modulations of the local shear were also shown to play a prominent role in introducing order unity changes to the marginal stability boundaries for infinite-n ideal ballooning instabilities. Since infinite-n ballooning stability boundaries are sometimes used as a proxy for the onset of virulent kinetic ballooning modes (KBM) [46–48], it can be argued that applied 3D fields can substantially alter KBM turbulence properties in the pedestal regime. What is shown in the present work is that 3D fields can also significantly modify trapped particle drifts and hence alter trapped particle instability properties. Moreover, the three-dimensional nature of the equilibrium produces a field line dependence to key physical quantities suggesting differing flux tubes on the same magnetic surface will have different micoinstability properties. Detailed quantification of the effects of 3D fields of microturbulence requires the use of gyrokinetic tools capable of using 3D MHD equilibrium that properly describes the shielding physics and plasma response associated with applied 3D fields.

ACKNOWLEDGMENTS

This work was supported by the U. S. Department of Energy under Grant nos. DE-FG02-86ER53218 and DE-SC0006103.

[1] A. H. Boozer, *Phys. Plasmas* **16**, 058102 (2009).
[2] J. D. Callen, *Nucl. Fusion* **51**, 094026 (2011).
[3] T. E. Evans, R. A. Moyer, P. R. Thomas, J. G. Watkins, T. H. Osborne, J. A, Boedo, E. J. Doyle, M. E. Fenstermacher, K. H. Finken, R. J. Groebner et al, *Phys. Rev. Lett.* **92**, 235003 (2004).
[4] Y. Liang, H. R. Koslowski, P. R. Thomas, E. Nardon, N. Alper, P. Andrew, Y. Andrew, G. Arnoux, Y. Barano, M. Becoulet et al, *Phys. Rev. Lett* **98**, 265004 (2007).
[5] A. Kirk, A. Nardon, R. Akers, M. Becoulet, G. De Temmerman, B. Dudson, B. Hnat, Y. Q. Liu, R. Martin, P. Tamain et al, *Nucl. Fusion* **50**, 034008 (2010).
[6] W. Suttrop, T. Eich, J. C. Fuchs, S. Guenter, A. Janzer, A. Herrmann, A. Kallenbach, P. T. Lang, T. Lunt, M. Maraschek et al, *Phys. Rev. Lett.* **106**, 225004 (2011(.
[7] Y. M. Jeon, J.-K. Park, S. W. Yoon, W. H. Lo, S. G. Lee, K. D. Lee, G. S. Yun, Y. U. Nam, W. C. Kim, jong-Gu Kwak et al, *Phys. Rev. Lett.* **109**, 035004 (2012).
[8] N. M. Ferraro, *Phys. Plasmas*, **19**, 056105 (2012).
[9] M. Becoulet, F. Orain, P. Maget, N. Mellat, X. Garbet, E. Nardon, G. T. A. Huysmans, T. Casper, A. Loarte, P. Cahyna et al, *Nucl. Fusion* **52**, 054003 (20120.
[10] Y. Q. Liu, A. Kirk, Y. Gribov, M. P. Gryaznevich, T. C. Hender and E. Nardon, *Nucl. Fusion* **51**, 083002 (2011).
[11] I. T. Chapman, M. Becoulet, T. M. Bird, J. Canik, M. Cianciosa, W. A. Cooper, T. Evans, N. Ferraro, C. Fuchs, M. Gryaznevich et al, *Nucl. Fusion* **54**, 083006 (2014).
[12] I. T. Chapman, W. A. Cooper, A. Kirk, C. J. Ham, J. R. Harrison, A. Patel, S. D. Pinches, R. Scannell, A. J. Thornton and the MAST team, *Plasma Phys. Control. Fusion* **54**, 105013 (2012).
[13] T. M. Bird and C. C. Hegna, *Nucl. Fusion* **53**, 013004 (2013).
[14] C. C. Hegna, *Phys. Plasmas* **21**, 072502 (2014).
[15] G. R. McKee, Z. Yan, C. Holland, R. J. Buttery, T. E.Evans, R. A. Moyer, S. Mordijck, R. Nazikian, T. L. Rhodes, O. Schmitz and M. R. Wade, *Nucl. Fusion* **53**, 113011 (2013).
[16] A. Skyman, H. Nordman and P. I. Strand, *Nucl. Fusion* **52**, 114015 (2012).
[17] A. Diallo, J. Canik, T. Göerler, S.-H. Ku, G. J. Kramer, T. Osborne, P. Snyder, D. R. Smith, W. Guttenfelder, R. E. Bell, D. P. Boyle, C.-S. Chang, B. P. LeBlance, R. Maingi, M. Podesta and S. Sabbagh, *Nucl. Fusion* **53**, 093026 (2013).
[18] D. R. Smith, S. E. Parker, W. Wan, Y. Chen, A. Diallo, B. D. Dudson, R. J. Fonck, W. Guttenfelder, G. R. McKee, S. M. Kaye, D. S. Thompson, R. E. Bell, B. P. LeBlance and M. Podesta, *Nucl. Fusion* **53** 113029 (2013).

[19] D. P. Fulton, Z. Lin, I. Holod and Y. Xiao, *Phys. Plasmas* **21**, 042110 (2014).

[20] D. R. Hatch, D. Told, F. Jenko, H. Doerk, M. G. Dunne, E. Wolfrum, E. Viezzer, The ASDEX Upgrade Team and M. J. Pueschel, *Nucl. Fusion* **55**, 063028 (2015).

[21] M. N. Rosenbluth, *Phys. Fluids* **11**, 869 (1968).

[22] B B. Kadomtsev and O. P. Pogutse, *Nucl. Fusion* **11**, 67 (1971).

[23] J. W. Connor, R. J. Hastie and T. J. Martin, *Nucl. Fusion* **23**, 1702 (1983).

[24] A. D. Turnbull, N. M. Ferraro, V. A. Izzo, E. A. Lazarus, J.-K. Park, W. A. Cooper, S. P. Hirshman, L. L. Lao, M. J. Lanctot, S. Lazerson, Y. Q. Liu, A. Reiman and F. Turco, *Phys. Plasmas* **20**, 056114 (2013).

[25] A. H. Reiman, N. M. Ferraro, A. Turnbull, J. K. Park, A. Cerfon, T. E. Evans, M. J. Lanctot, E. A. Lazarus, Y. Liu and G. McFadden, *Nucl. Fusion* **55**, 063026 (2015).

[26] C. C. Hegna, *Phys. Plasmas* **7**, 3921(2000).

[27] A. H. Boozer, *Phys. Plasmas* **9**, 3762 (2002).

[28] R. L. Miller, M. S. Chu, J. M. Greene, Y. R. Lin-Liu and R. E. Waltz, *Phys. Plasmas* **5**, 973 (1998).

[29] N. Nakajima, S. R. Hudson, C. C. Hegna and Y. Nakamura, *Nucl. Fusion* **46**, 177 (2006).

[30] M. Hirsch, J. Baldzuhn, C. Beidler, R. Brakel, R. Burhenn, A. Dinklage, H. Ehmler, M. Endler, V. Erckmann, Y. Feng, J. Geiger, et al *Plasma Physics and Controlled Fusion* **50**, 053001 (2008).

[31] T. M. Bird and C. C. Hegna, *Phys. Plasmas* **21**, 100702 (2014).

[32] C. C. Hegna and N. Nakajima, *Phys. Plasmas* **5**, 1336 (1998).

[33] C. C. Hegna and S. R. Hudson, *Phys. Rev. Lett.* **87**, 035001 (2001).

[34] J. L. V. Lewandowski, *Phys. Plasmas* **10**, 4053 (2003).

[35] M. N. Rosenbluth and M. L. Sloan, *Phys. Fluids* **14**, 1725 (1971).

[36] R. J. Dewar and A. H. Glasser, *Phys. Fluids* **26**, 3038 (1983).

[37] G. Rewoldt, L. P. Ku, and W. M. Tang, *Phys. Plasmas* **12**, 102512 (2005).

[38] T. Rafiq and C. C. Hegna, *Phys. Plasmas* **13**, 062501 (2006).

[39] J. H. E. Proll, P. Helander, J. W. Connor, and G. G. Plunk, *Phys. Rev. Lett.* **108** 245002 (2012).

[40] B. J. Faber, M. J. Pueschel, J. H. E. Proll, P. Xanthopoulos, P. W. Terry, C. C. Hegna, G. M. Weir and J. N. Talmadge, *Phys. Plasmas* **22**, 072305 (2015).

[41] H. Sugama and T. H. Watanabe, *Phys. Plasmas* **13**, 012501 (2006).

[42] J.-K. Park, A. H. Boozer and J. E. Menard, *Phys. Rev. Lett.* **102**, 065002 (2009).

[43] K. C. Shaing, S.A. Sabbagh and M. S. Chu, *Plasma Phys. and Control. Fusion* **51**, 075015 (2009).

[44] M. Landerman and P. J. Catto, *Plasma Phys. Control. Fusion* **53**, 015004 (2011).

[45] K. C.Shaing, S. A. Sabbagh and M. S. Chu, *Nuclear Fusion* **50**, 025022 (2010) and references therein.

[46] P. B. Snyder and G. W. Hammett, *Phys. Plasmas* **8**, 744 (2001).

[47] M. J. Pueschel, M. Kammerer and F. Jenko, *Phys. Plasmas* **15**, 102310 (2008).

[48] E. A. Belli and J. Candy, *Phys. Plasmas* **17**, 112314 (2010).